Volume 53
Number 40
28 October 2024
Pages 16425-16760

Dalton Transactions

An international journal of inorganic chemistry

rsc.li/dalton

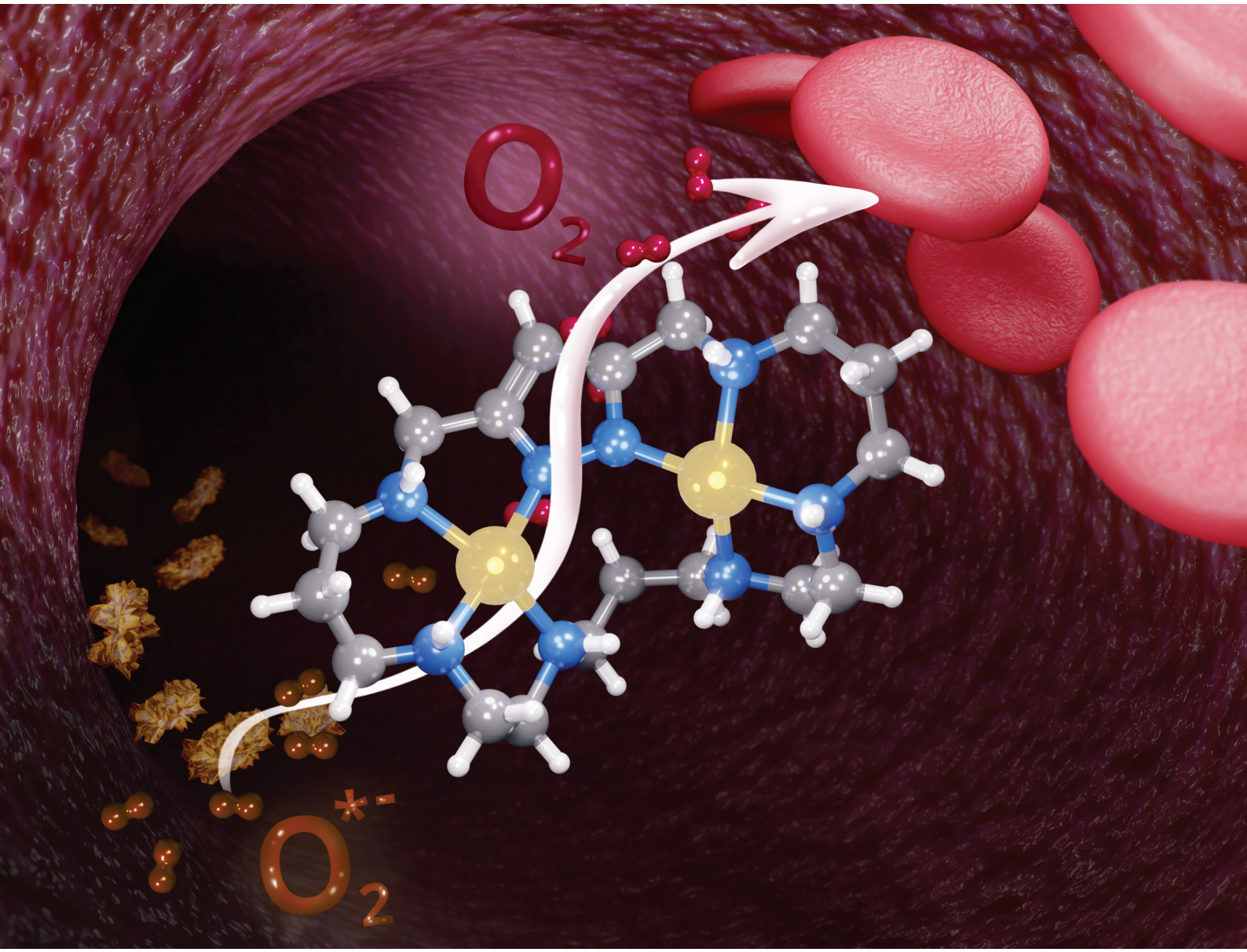

ISSN 1477-9226

PAPER

Enrique García-España, M. Paz Clares *et al.*
Exo- or endo-1*H*-pyrazole metal coordination modulated by the polyamine chain length in [1 + 1] condensation azamacrocycles. Binuclear complexes with remarkable SOD activity

ROYAL SOCIETY OF CHEMISTRY

Dalton Transactions

ROYAL SOCIETY OF CHEMISTRY

PAPER

View Article Online
View Journal | View Issue

Cite this: *Dalton Trans.*, 2024, **53**, 16480

Exo- or endo-1*H*-pyrazole metal coordination modulated by the polyamine chain length in [1 + 1] condensation azamacrocycles. Binuclear complexes with remarkable SOD activity†

Irene Bonastre-Sabater,[a] Alberto Lopera,[a] Álvaro Martínez-Camarena,[a,b] Salvador Blasco,[a] Antonio Doménech-Carbó,[c] Hermas R. Jiménez,[d] Begoña Verdejo,[a] Enrique García-España *[a] and M. Paz Clares *[a]

The Cu^{2+} complexes of three [1 + 1] azacyclophane macrocycles having the 1*H*-pyrazole ring as the spacer and the pentaamine 1,5,8,11,15-pentaazadecane (**L1**) or hexaamines 1,5,8,12,15,19-hexaazanonadecane (**L2**) and 1,5,9,13,17,21-hexaazaheneicosane (**L3**) as bridges show endo- coordination of the pyrazolate bridge giving rise to discrete monomeric species. Previously reported pyrazolacyclophanes evidenced, however, exo-coordination with the formation of dimeric species of 2 : 2, 3 : 2 or even 4 : 2 Cu^{2+} : L stoichiometry. The complexes have been characterized in solution using potentiometric studies, UV-Vis spectroscopy, paramagnetic NMR, cyclic voltammetry and mass spectrometry. The measurements show that all three ligands have as many protonation steps in water as secondary amines are in the bridge, while they are able to form both mono- and binuclear Cu^{2+} species. The crystal structures of the complexes $[Cu(H\mathbf{L1})Br]Br_{(1+x)}(ClO_4)_{(1-x)}\cdot yH_2O$ (**1**) and $[Cu_2(H_{-1}\mathbf{L2})Cl(ClO_4)](ClO_4)\cdot H_2O\cdot C_2H_5OH$ (**2**) have been solved by X-ray diffraction studies. In **1** the metal ion lies at one side of the macrocyclic cavity being coordinated by one nitrogen of the pyrazolate moiety and the three consecutive nitrogen atoms of the polyamine bridge. The other nitrogen of the pyrazole ring is hydrogen-bonded to an amine group. In **2** the two metal ions are interconnected by a pyrazolate bis(monodentate) moiety and complete their coordination spheres with three amines and either a bromide or a perchlorate anion, which occupy the axial positions of distorted square pyramid geometries. Paramagnetic NMR studies of the binuclear complexes confirm the coordination pattern observed in the crystal structures. Cyclic voltamperommetry data show potentials within the adequate range to exhibit superoxide dismutase (SOD) activity. The IC_{50} values calculated by McCord–Fridovich enzymatic assays show that the binuclear Cu^{2+} complexes of **L2** and **L3** have SOD activities that rank amongst the highest ones reported so far.

Received 26th April 2024,
Accepted 27th June 2024

DOI: 10.1039/d4dt01236d

rsc.li/dalton

Introduction

1*H*-Pyrazole is an imidazole isomer that displays different hydrogen bond and coordination modes.[1] Among the latter, the most relevant ones are monodentate coordination in its neutral form and bis(monodentate) or exo(bidentate) coordination in its deprotonated pyrazolate form. These coordination and hydrogen bond features have made pyrazole and its derivatives, particularly carboxylates, well-known building blocks in the preparation of metal–organic frameworks (MOFs).[2,3] On the other hand, pyrazole and its derivatives have found interesting applications in pharmacology.[4]

The bis(monodentate) coordination mode of the pyrazolate anion separates the metal ions from 3.7 to 4.0 Å, distances which are close to those found in type III copper centres of biomolecules such as hemocyanin or multinuclear copper

[a]*Departamento de Química Inorgánica, Instituto de Ciencia Molecular. Universidad de Valencia, Calle Catedrático José Beltrán 2, 46980 Paterna, Valencia, Spain. E-mail: m.paz.clares@uv.es, enrique.garcia-es@uv.es*
[b]*Departamento de Química Inorgánica, Facultad de Ciencias Químicas, Universidad Complutense de Madrid, avda. Complutense s/n, 28040 Madrid, Spain*
[c]*Departamento de Química Analítica, Universidad de Valencia, Calle Dr Moliner s/n, 46100 Burjassot, Valencia, Spain*
[d]*Departamento de Química Inorgánica, Universidad de Valencia, Calle Doctor Moliner s/n, 46100 Burjasot, Valencia, Spain*

†Electronic supplementary information (ESI) available: Text figures, tables, and physical measurements. CCDC 2240668 and 2215780. For ESI and crystallographic data in CIF or other electronic format see DOI: https://doi.org/10.1039/d4dt01236d

enzymes.[5] In this respect, several 1*H*-pyrazole open-chain ligands and complexes have been prepared to mimic enzymes or to analyse the electronic and magnetic properties of the interconnected metal ions.[6]

Previously, others and we have extensively worked on the synthesis and study of [2 + 2] condensation macrocycles in which two 1*H*-pyrazole units were bound through methylene groups to different polyamine chains.[7] This work was also extended to [3 + 2] condensation cryptands in which three pyrazole spacers were linked to two tris(2-aminoethyl)amine (*tren*) moieties or analogue tripodal polyamines. These macrocycles showed interesting behaviours regarding their metal and anion coordination, biomedical chemistry and self-assembling properties. [2 + 2] Azamacrocycles proved to have strong binding to metal ions, amino acids and neurotransmitters.[8] Interestingly, the interaction of a [2 + 2] macrocycle having cadaverine polyamines with Cu^{2+} led to the formation of a 4 : 2 Cu^{2+} : ligand metallocage appropriately sized to host a water molecule that seemed not be hydrogen bonded to any other water molecule or to donor or acceptor groups within the cage.[9]

The cryptand containing *tren* units was able to encapsulate metal ions and different anions within its cavity as proved by a variety of techniques including single crystal X-ray diffraction.[10] The combination of the pyrazole bis(monodentate)-binding motif and polyamine organization permitted interesting Cu^{2+}-cryptand cages to be obtained in which six metal ions were shared by three cryptands through a right arrangement of the amines in axial positions.[11] Moreover, we noticed that by regulating the pH we could reach a situation in which the protonated amino groups of the cryptand selectively hosted chloride anions and water molecules, while the pyrazole groups coordinated in an exo-monodentate fashion with Cu^{2+} ions linking cryptand moieties so that a 1D-helical coordination polymer behaving as a multi-anion receptor was formed.[12]

In spite of all this interest in [2 + 2] 1*H*-pyrazole macrocycles, the number of research works dealing with [1 + 1] condensation of 1*H*-pyrazole azamacrocycles is much more scarce. As far as we know, after a previous report showing the synthesis and characteristics of a series of 1*H*-pyrazole oxygen crown ethers as dopamine receptors,[13] only three papers coming from our own laboratory have appeared describing [1 + 1] 1*H*-pyrazole azamacrocycles.[14–16] These papers revealed that the binding of a single 1*H*-pyrazole to the ends of different open-chain tetra-amines to produce [1 + 1] azamacrocycles gave rise to Cu^{2+} complexes with exo-coordination of the 1*H*-pyrazole fragments so that complexes of 2 : 2, 3 : 2 and even 4 : 2 Cu^{2+} : ligand stoichiometry were predominantly formed as assessed by solution studies and X-ray diffraction (Fig. 1). The ability of pyrazole to show an exo-binding mode was very nicely illustrated in the case of macrocycles formed by pyrazole and imidazole units whose Cu^{2+} complexes led to pillared structures.[17] In none of these systems, discrete binuclear 2 : 1 Cu^{2+} complexes were detected. However, such binuclear metal complexes, in particular the Cu^{2+} ones, may have great relevance in biomimetic chemistry. As mentioned above, the positioning of the Cu^{2+} atoms at the *ca.* 3.7 Å distance dictated by

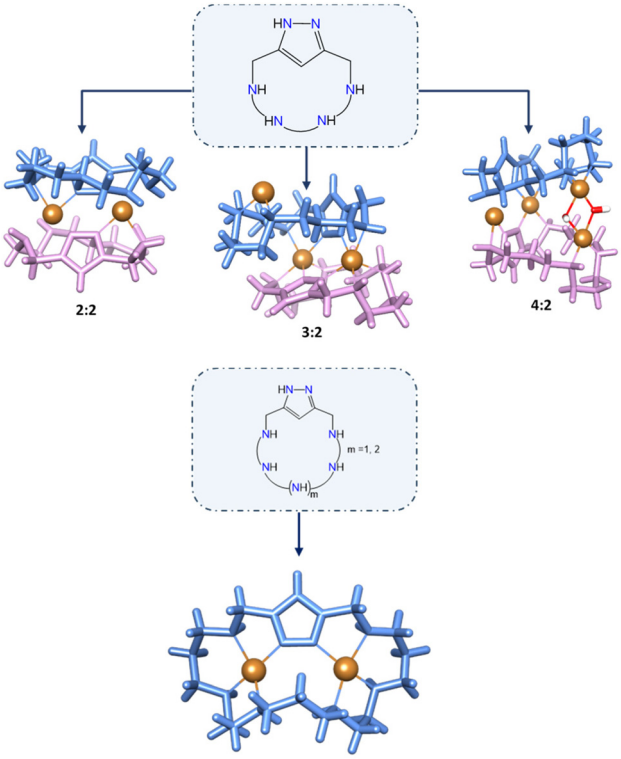

Fig. 1 Coordination modes in [1 + 1] condensation polyazapyrazolaphanes.

the bis(monodentate) pyrazolate anion may have relevance for instance in the mimicking of enzymes involved in the protection against reactive oxygen species (ROS). The so far explored [2 + 2] 1*H*-pyrazole condensation macrocycles saturate the space between the metal ions making difficult their transient binding to exogenous ligands as the superoxide radical or hydrogen peroxide anions involved in these processes.

Regarding this point, our group has been synthesizing and studying pyridinaphane macrocyclic receptors whose copper or manganese complexes had the capacity to scavenge superoxide radical anions promoting their disproportionation into hydrogen peroxide and dioxygen. In particular, mononuclear manganese complexes of tetraazapyridinaphane ligands having pending polyamine chains and binuclear copper complexes of hexaazapyridinaphane macrocycles have shown interesting superoxide dismutase (SOD) mimicking potentiality *in vitro* (see Fig. 2).[18,19]

Moreover, we have reported that grafting of the active amines onto boehmite nanoparticles (γ-AlO(OH), BNPs) giving rise to amino-nanozyme systems led to a significant activity increase due to the positive charge of the BNPs and accumulation of the complexes on the surface.[20,21] Literature reports show interesting properties in imaging and in therapeutic intervention against Alzheimer's disease of metal complexes of the derivatives of the molecule 3,6,9-triaza-1-(2,6)-pyridinacyclodecaphane (py22 or pyclen), which constitutes the macrocyclic core of our pending pyridinaphane ligands.[22] In this line, we have recently shown that the Cu^{2+} complexes of a py22 derivative with a carboxylate

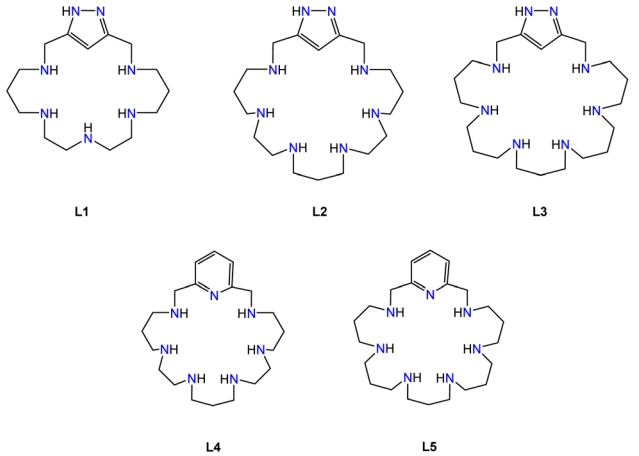

Fig. 2 Ligand drawing.

group at the *para* position developed a striking SOD activity, while when grafted to BNPs amino-nanozymes were obtained displaying mitoROS scavenging properties and the ability to disaggregate mutant huntingtin deposits in cells.[23]

As mentioned above, in this work, we turn our attention towards macrocyclic polyamines and we want to learn how replacing the pyridine aromatic spacer by a 1*H*-pyrazole one influences the superoxide dismutase activity in 2 : 1 Cu^{2+} : macrocycle binuclear systems. It has been shown that the way in which superoxide anions approach and bind to the active centre of the enzyme is a key factor in the catalytic cycle. Since the 1*H*-pyrazole spacer has the possibility to donate and accept hydrogen bonds, it may have some relevant effect on the catalysis of superoxide disproportionation.[24] In this context, here we report on the Cu^{2+} complexes of the newly synthesized ligand 3,7,10,13,17-pentaaza-1-(3,5)-pyrazolacyclooctadecaphane (**L1**) and their potential capability to behave as superoxide dismutase mimics. Moreover, we have extended these studies to the 1*H*-pyrazole hexaaza-macrocycles 3,7,10,14,17,21-hexaaza-1-(3,5)-pyrazolacyclodocosaphane and 3,7,11,15,19,22-hexaaza-1-(3,5)-pyrazolacyclotetracosaphane, hereafter (**L2**) and (**L3**). We have used penta- and hexaamines in the bridges to avoid exo-binding to metal ions of the 1*H*-pyrazole unit and to permit endo coordination facilitating the formation of monomeric binuclear complexes involving just one macrocycle. We have used a handful of experimental techniques to establish the acid–base and Cu^{2+} coordination chemistry in solution of the three ligands and we describe the crystal structure of the mononuclear complex $[Cu(H\mathbf{L1})Br]Br_{(1+x)}(ClO_4)_{(1-x)}\cdot yH_2O$ (**1**) and the binuclear one $[Cu_2(H_{-1}\mathbf{L2})Cl(ClO_4)](ClO_4)\cdot H_2O\cdot C_2H_5OH$ (**2**).

Results and discussion

Synthetic procedures

The synthesis of **L1** was carried out employing the modification of the Richman–Atkins procedure[25] we had previously used for the synthesis of **L2** and **L3**, and related tetraaza pyrazolacyclophanes.[14–16] The procedure comprises the cyclisation reaction between the protected pyrazole moiety 3,5-bis (chloromethyl)-1-(tetrahydropyran-2-yl)-pyrazole and the corresponding tosylated pentaamine followed by the removal of the protecting groups in acid media using a hydrobromide/acetic acid mixture and phenol (Scheme 1). Protection of the pyrazole group is necessary to avoid side-reactions.[26]

Acid–base behaviour

Table 1 shows the stepwise and cumulative protonation constants of **L1**, **L2** and **L3** determined by means of pH-metric titrations employing the HYPERQUAD software.[27] Distribution diagrams calculated with the program HySS[28] are collected in the ESI (Fig. S1–S3†). As shown in Table 1, the macrocycles display in the pH range available for potentiometric titrations (2.5–11.0) as many constants as the number of secondary amine groups present in their structures.

As observed in previous related systems neither protonation nor deprotonation of the 1*H*-pyrazole units occurs within the explored pH range.[7,29,30] For the three macrocycles, the values of the logarithms of the protonation constants decrease as the number of positive charges in the receptor increases, following the expected trend for polyazamacrocycles, which can be ascribed to an increase of the electrostatic repulsions between the positively charged protonated amines.[31] **L3** has, in general, higher basicity than **L2** in all the protonation steps, while **L1** has less basicity in all of them. Similar trends were obtained for pyridinaphanes with analogous polyaminic bridges.[19] The greater number of carbon atoms between the secondary amino groups in **L3** leads to larger inductive effects and to a greater minimization of electrostatic repulsions between the charged ammonium groups, resulting in higher stepwise protonation constants.[31] As a matter of fact, **L3** presents six orders of mag-

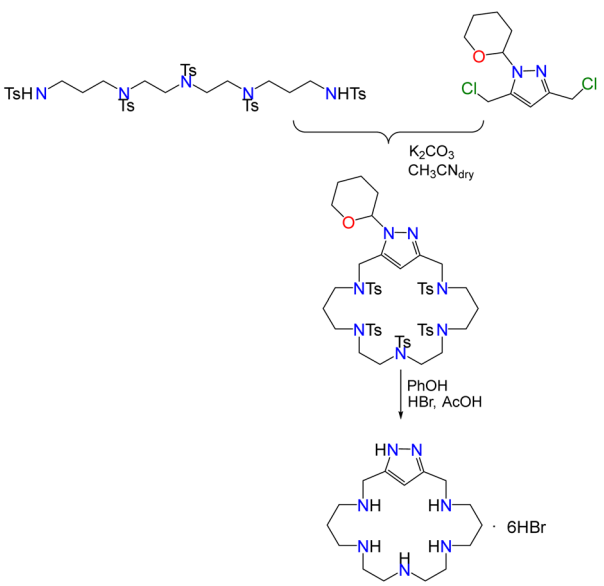

Scheme 1 Ligand synthesis.

Table 1 Logarithms of the stepwise protonation constants of **L1**, **L2** and **L3** determined in 0.15 M NaCl at 298.1 ± 0.1 K

Reaction[a]	L1	L2	L3
L + H ⇄ HL	9.61(2)[b]	10.06(1)[c]	10.72(1)[c]
HL + H ⇄ H_2L	9.26(2)	9.24(1)	9.80(1)
H_2L + H ⇄ H_3L	7.35(3)	8.09(1)	8.63(1)
H_3L + H ⇄ H_4L	6.35(3)	6.50(1)	7.46(1)
H_4L + H ⇄ H_5L	3.09(3)	5.41(1)	6.90(1)
H_5L + H ⇄ H_6L	—	4.42(2)	6.02(1)
log β[d]	35.66(3)	43.72(2)	49.53(1)

[a] Charges omitted. [b] Numbers in parenthesis are standard deviation in the last significant figure. [c] Taken from ref. 16. [d] Calculated as $\log\beta = \Sigma_j \log K_{HjL}$.

nitude greater overall basicity than **L2** (see the last entry in Table 1). The variations of the pyrazole UV band at *ca.* 205 nm with the pH value indicate that the amine groups closer to the pyrazole moieties are the first ones being protonated, since from pH 9 downwards no changes in absorptivity occur (see Fig. S1–S3 in the ESI†).

Cu^{2+} coordination

The stability constants of the Cu^{2+} complexes of the pyrazole cyclophanes **L1**, **L2** and **L3** have been obtained by potentiometric titration using the HYPERQUAD set of programs for the analysis of the data (Table 2).[27] Distribution diagrams have been produced with the program HySS (Fig. 3, Fig. S4 and S5†).[28] The titrations were carried with Cu^{2+} : L molar ratios from 1 : 2 to 2 : 1 in the pH range 2.5–11.0. **L1**, **L2** and **L3** form mono- and binuclear monomeric complexes of $[Cu(H_xL)]^{(2+x)+}$ or $[Cu_2(H_yL)]^{(4+y)+}$ stoichiometries. For **L1** the x and y values range from 2 to 1 and from −1 to −3, respectively. For **L2** and **L3**, x varied from 3 to −1 and from 4 to −1, respectively, while x changed from 0 to −2 for both systems.

Table 2 Logarithms of the stability constants for the Cu^{2+}–**L1**, Cu^{2+}–**L2** and Cu^{2+}–**L3** systems, determined in 0.15 M NaCl at 298.1 ± 0.1 K

Reaction[a]	L1	L2	L3
Cu + L + 4H ⇄ CuH_4L			43.71(3)
Cu + L + 3H ⇄ CuH_3L		38.04(4)	38.97(4)
Cu + L + 2H ⇄ CuH_2L	30.49(2)[b]	34.82(2)	34.42(1)
Cu + L + H ⇄ CuHL	27.03(1)	30.77(4)	28.21(2)
Cu + L ⇄ CuL	19.63(3)	22.56(5)	19.23(3)
Cu + L ⇄ $CuH_{-1}L$ + H	9.21(4)	11.15(6)	8.62(3)
2Cu + L ⇄ $Cu_2(H(H_{-1}L))$		30.44(6)	28.00(4)
2Cu + L ⇄ $Cu_2(H_{-1L})$ + H	20.50(2)	26.68(2)	23.20(1)
2Cu + L ⇄ $Cu_2(H_{-1}L)(OH)$ + 2H	13.20(3)	16.58(4)	11.95(4)
2Cu + L ⇄ $Cu_2(H_{-1}L)(OH)_2$ + 3H	2.84(4)		
CuH_3L + H ⇄ CuH_4L			4.74(3)
CuH_2L + H ⇄ CuH_3L		3.21(3)	4.55(4)
$Cu(H_2(H_{-1}L))$ + H ⇄ CuH_2L	3.46(2)	4.06(4)	6.20(2)
$Cu(H(H_{-1}L))$ + H ⇄ $Cu(H_2(H_{-1}L))$	7.40(3)	8.20(4)	8.98(2)
$Cu(H_{-1}L)$ + H ⇄ $Cu(H(H_{-1}L))$	10.41(5)	11.41(7)	10.61(4)
Cu + $Cu(H(H_{-1}L))$ ⇄ $Cu_2(H_{-1}(HL))$		7.87(7)	8.77(5)
$Cu_2(H(H_{-1}L))$ ⇄ $Cu_2(H_{-1}L)$+ H		−3.76(6)	−4.80(4)
$Cu_2(H_{-1}L)$ + H_2O ⇄ $Cu_2(H_{-1}L)(OH)$ + H	−7.30(2)	−10.10(4)	−11.25(4)
$Cu_2(H_{-1}L)(OH)$ ⇄ $Cu_2(H_{-1}L)(OH)_2$ + H	−10.36(5)		

[a] Charges omitted. [b] Numbers in parenthesis are standard deviation in the last significant figure.

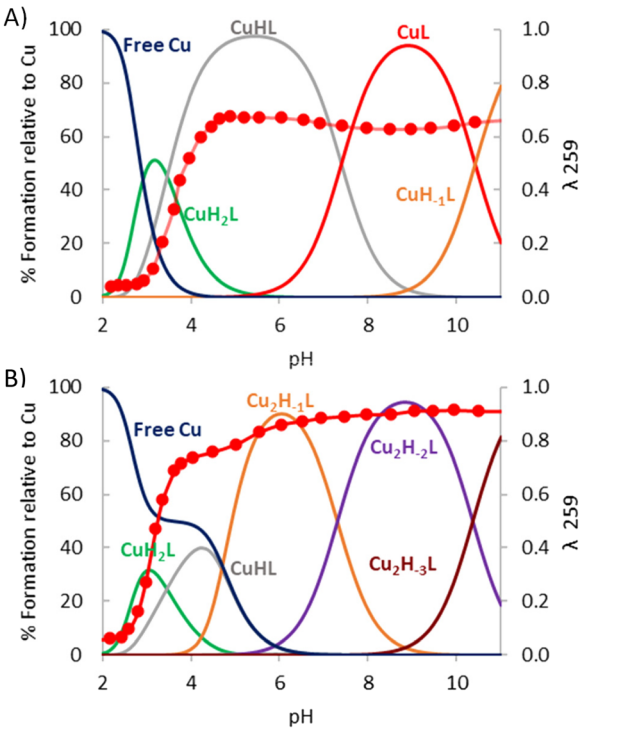

Fig. 3 Distribution diagram for the system Cu^{2+}–**L1** overlapped with the absorbance at 259 nm [**L1**] = 1 × 10^{-3} M, (A) [Cu^{2+}] = 1 × 10^{-3} M and (B) [Cu^{2+}] = 2 × 10^{-3} M.

HR-ESI-MS studies, performed at variable pH, permitted the identification of most of the species detected in the potentiometric studies, confirming their mono- and binuclear nature (Table 3). Fig. S6–S28† show the experimental and calculated spectra for the detected species.

In contrast to related shorter derivatives having tetraamine bridges,[14,15] which showed the formation of dimeric bi-, tri or tetranuclear complexes (Cu^{2+} : L stoichiometries 2 : 2. 3 : 2 or 4 : 2) (Fig. 1), for **L1**, **L2** and **L3** we have only been able to detect mono- and binuclear monomeric complexes. The larger size and number of amine groups, along with the greater flexibility of these ligands, permit an enough number of nitrogen donors to point inside their cavities, giving rise to an endo-coordination instead of the preferred exo-coordination mode observed for the parent tetraamine pyrazole macrocycles.[14,15]

The formation of discrete binuclear complexes for **L1** and **L3** has also been checked by paramagnetic NMR spectroscopy. We have recorded the ^{1}H NMR spectra, measured the ^{1}H transversal relaxation times, T_2, and analysed the temperature dependence of the chemical shifts. The ^{1}H NMR spectrum of the system Cu^{2+}–**L1** in a 2 : 1 molar ratio recorded in D_2O at pH = 7 shows, in the downfield region, five well-resolved isotropically shifted signals (a–c, f and g) and three signals (d), (e) and (E). In addition, it displays four signals (h–k) shifted upfield (Fig. S29†). Chemical shift values, linewidths at half-height, transversal relaxation time values (T_2) and assignments are reported in the ESI (Table S1†). The assignment of the isotropi-

Table 3 Experimental and calculated *m*/*z* peaks found for the mono- and binuclear Cu^{2+}–**L1**, Cu^{2+}–**L2** and Cu^{2+}–**L3** systems by ESI-MS

	L1		L2		L3	
Ligand Species	Found	Calculated	Found	Calculated	Found	Calculated
$[CuL]^{2+}$	186.0950	186. 1018	214.6258	214.6252	228.6411	228.6401
$[CuL(Cl)]^{+}$	407.1608	407.1725	464.2193	462.2199	492.2513	492.2512
$[CuL(ClO_4)]^{+}$	417.1433	417.1522	528.1984	528.1995	556.2309	556.2308
$[CuH_{-1}L]^{+}$	371.1837	371.1959	—	—	456.2742	456.2745
$[Cu_2H_{-1}L(Cl)]^{2+}$	—	—	263.0712	263.0705	277.0871	277.0862
$[Cu_2H_{-1}L(ClO_4)]^{2+}$	—	—	295.0610	295.0604	309.0775	309.0760
$[Cu_2H_{-2}L]^{2+}$	216.5522	216.5638	245.0833	245.0822	259.0992	259.0979
$[Cu_2H_{-2}L(Cl)]^{+}$	470.0763	470.0965	525.1331	525.1338	553.1654	553.1651
$[Cu_2H_{-2}L(ClO_4)]^{+}$	—	—	589.1125	589.1135	617.1452	617.1448

cally shifted signals, as well as the description of the characteristic properties of the binuclear Cu^{2+} system have been performed taking into account previous reports.[15,32]

The isotropically shifted signals show linewidths, measured at half-height, of around ~70 Hz, except for signals a–c and h–k with a linewidth of 2960 to 850 Hz, respectively. Transversal relaxation time values were below 1 ms, in the case of signals a–c and h–k, and 4 ms for signals f and g. The assignments of the isotropically shifted signals by means of the integration of signals and the transversal relaxation times of the paramagnetic signals are shown in Table S1.† Chemical shift values, transversal relaxation times and the broad linewidth at half-height of the Cu^{2+}–**L1** system in 2 : 1 molar ratio are characteristic of a spin-coupled binuclear Cu^{2+}.[15,19,32,33] The pattern of paramagnetic signals for the macrocyclic protons supports the formation of monomeric binuclear complexes with the nitrogen coordination pattern shown in Scheme 2.

The paramagnetic ^{1}H NMR spectrum of the system Cu^{2+}–**L3** for 2 : 1 molar ratio in D_2O at 298 K and pH = 6 is shown in Fig. S30.†

The hyperfine-shifted resonances, linewidth at half-height and T_2 values are reported in Table S2.† The pattern of paramagnetic signals for this system also suggests in this case the formation of monomeric binuclear complexes in which the metal centres are bound to four nitrogen atoms as represented in Scheme 2.

Variable temperature ^{1}H NMR spectra of both systems were recorded from 283 to 323 K. Isotropically shifted signals are temperature dependent following a Curie behaviour except for some signals belonging to β-CH_2 or H_mPz protons of the macrocyclic ligand that show an anti-Curie or temperature independent behaviour. In the Curie behaviour the paramagnetically shifted signals decrease with increasing temperature (see Tables S1 and S2†). The anti-Curie dependence results are indicative of spin-coupled dicopper(II) systems with antiferromagnetic coupling.

An interesting point concerns the actual protonation degree of the pyrazole moiety. As previously mentioned, 1*H*-pyrazole may either bind a proton behaving as a base or deprotonate to give the pyrazolate anionic form. In the absence of metal ions, these equilibria occur either at very acidic or very basic pH values falling outside the pH range of the technique.[29,30]

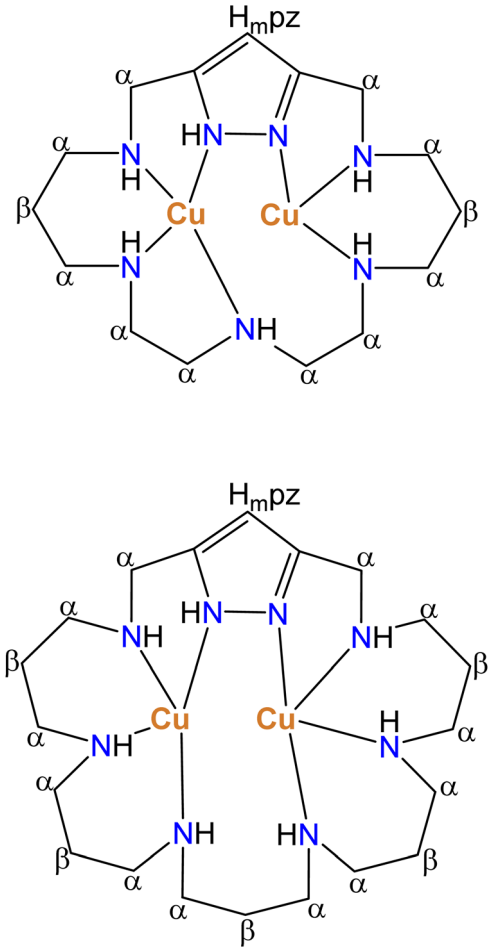

Scheme 2 Nitrogen coordination pattern found in binuclear Cu^{2+} complexes of **L1** and **L3** suggested by paramagnetic ^{1}H NMR spectra.

Formation of binuclear complexes induces the ready deprotonation of pyrazole to give rise to the preferred bis(monodentate) binding mode of this unit.[10,11] However, a point that has not yet been fully addressed is the protonation state of pyrazole in the case of formation of mononuclear complexes, although the two nitrogen atoms of the pyrazole moiety can very hardly converge into a single metal ion since the formation of a three-

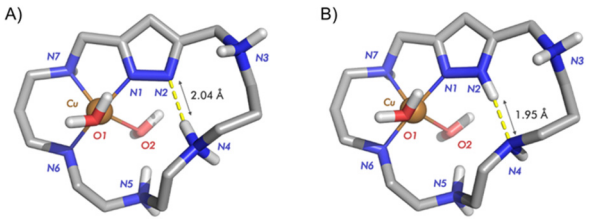

Fig. 4 Representation of the most stable structure for the monoprotonated Cu^{2+}–**L1** complex. (A) $[Cu(H_2(H_{-1}\mathbf{L1})]^{3+}$ and (B) $[Cu(H\mathbf{L1})]^{3+}$. Structure B is *ca.* 8.8 kJ mol^{-1} more stable than A.

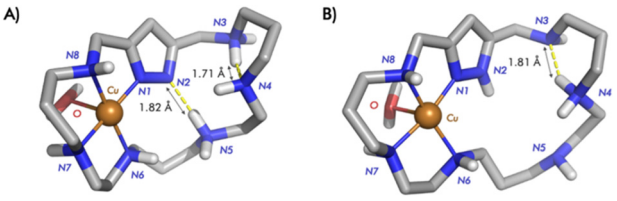

Fig. 6 Representation of the most stable structure for the monoprotonated Cu^{2+}–**L2** complex. (A) $[Cu(H_2(H_{-1}\mathbf{L2})]^{4+}$ and (B) $[Cu(H\mathbf{L2})]^{4+}$. Structure B is *ca.* 25.3 kJ mol^{-1} more stable than A.

membered chelate ring would be required. To shed some light on this aspect, we have recorded the variation with the pH of the UV spectra for all three systems both in 1 : 1 and 2 : 1 Cu^{2+} : L molar ratios and the corresponding plots are given in Fig. 4A and B for **L1** and in Fig. S4 and S5† for **L2** and **L3**. Fig. 3A, which shows the distribution diagrams *versus* pH for the system Cu^{2+} : **L1** in a 1 : 1 molar ratio overlapped with the absorbance of pyrazole at 247 nm, shows that the formation of the mononuclear complexes at pH 3–4 produces an increase in the absorbance which reaches a plateau and remains thereon constant. The formation of binuclear complexes (Fig. 3B) produces a further increase of absorbance of about 20%. Since in binuclear complexes the pyrazole is deprotonated, one might think that the binding of the first metal ion already polarizes the N–H bond of pyrazole to a considerable extent, polarization that would be assisted by hydrogen bonding with an amine group. Interestingly, calculations about the location of the residual electron density around the pyrazole in the crystal structure of the mononuclear complex $[Cu(H\mathbf{L1})Br]Br_{(1+x)}(ClO_4)_{(1-x)}{\cdot}yH_2O$ (**1**) (*vide infra*) show that the residual electron density of the proton would be at about 80% located in the amine group and 20% in the pyrazole nitrogen (see below).

This indicates the formation of a relatively strong hydrogen bond with proton transfer from the pyrazole to the amine group. DFT calculation about the mono- and diprotonated species assuming that the proton is either in the polyamine chain or in the pyrazole ring, for the monoprotonated species (A) $[Cu(H_2(H_{-1}\mathbf{L1})]^{3+}$ or (B) $[Cu(H\mathbf{L1})]^{3+}$ (Fig. 4), and for the diprotonated species (A) $[Cu(H_3(H_{-1}\mathbf{L1})]^{4+}$ and (B) $[Cu(H_2\mathbf{L1})]^{4+}$ (Fig. 5), reveals close energies between both structures, in both cases the structures with the proton located in the pyrazole ring being slightly favoured.

Similar calculations were performed for the diprotonated complex of **L2**, structures (A) $[Cu(H_2(H_{-1}\mathbf{L2})]^{4+}$ and (B) $[Cu(H\mathbf{L2})]^{4+}$ as shown in Fig. 6. The calculations denote a greater stabilisation of the structure in which the proton is placed at the pyrazole ring (structure B). In this case, the data do not suggest hydrogen bond formation between the pyrazole and the amine group in structure B, whereas hydrogen bonding is observed between protonated and non-protonated amines in the chain. In this structure hydrogen bonding is observed both within the chain and between the pyrazole N–H and an amine group of the chain.

Therefore, all the data seem to suggest that coordination of a single metal ion does not induce neat deprotonation of the pyrazole ring, even though hydrogen bonding with adjacent amine groups of the polyamine chain may contribute to the stabilisation of the structure.

Distribution diagrams in Fig. 3 for the system Cu^{2+}–**L1** and in Fig. S4 and S5† for the systems Cu^{2+}–**L2** and Cu^{2+}–**L3** show that the formation of mono- or binuclear complexes is clearly controlled by the Cu^{2+} : L molar ratio used. In all three systems for 1 : 1 molar ratio only mononuclear complexes form, while for 2 : 1 molar ratio binuclear complexes prevail in a broad pH window. In the case of the systems Cu^{2+}–**L2** and Cu^{2+}–**L3** for 2 : 1 molar ratio the species $[Cu_2(H_{-1}L)]^{2+}$ predominates from pH values of *ca.* 4 and 5 to 10 and 11, respectively. **L2** due to its hydrocarbon sequence will provide alternate 5- and 6-membered chelate rings favouring a stronger interaction with the metal ions than the only 6-membered chelate ring sequence of **L3**.[34] Consequently, in the Cu^{2+}–**L2** binuclear system the pyrazole is more strongly polarized and its deprotonation occurs at more acidic pH values. The structure of the $[Cu_2(H_{-1}L)]^{3+}$ species of **L2** and **L3** should essentially correspond to that observed for crystals **2** discussed in the next section. Next deprotonation to give $[Cu_2(H_{-1}L)(OH)]^{2+}$ would likely imply the loss of a proton by a coordinated water molecule. The values of the pK_as of these processes of 10.10 and 11.25 log units found for **L2** and **L3** (Table 2), respectively, suggest that the OH^- formed is not bridging both metal centres.

The system Cu^{2+}–**L1**, even though related, has several particularities as there is the absence of a $[Cu_2(H(H_{-1}L))]^{4+}$ species and the formation of both mono- and bis(hydroxylated) binuclear species. The pK_a obtained for the formation of the first

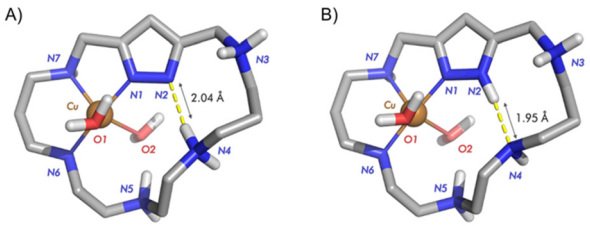

Fig. 5 Representation of the most stable structure for the diprotonated Cu^{2+}–**L1** complex. (A) $[Cu(H_3(H_{-1}\mathbf{L1})]^{4+}$ and (B) $[Cu(H_2\mathbf{L1})]^{4+}$. Structure B is *ca.* 1.0 kJ mol^{-1} more stable than A.

hydroxylated species $[Cu_2(H_{-1}\mathbf{L1})(OH)]^{2+}$ (pK_a = 7.30) may imply that the hydroxide formed is bridging both metal centres.[35] However the pK_a for the formation of the second one (pK_a = 10.36) suggests again that this step corresponds to the deprotonation of a coordinated water molecule without giving rise to the formation of a bridging hydroxide ligand. Electronic spin resonance (esr) spectra, recorded at the pH values where the maximum formation of the mononuclear and binuclear complexes occur, somehow support the formation of hydroxide bridging ligands in the binuclear complexes of **L1**. While the formation of the different 1 : 1 complexes (Fig. S31†) provides a signal for high spin monomeric Cu^{2+} that practically does not change with pH, the signal corresponding to the $[Cu_2(H_{-1}\mathbf{L1})]^{3+}$ species (pH = 6) (Fig. S32†) shows a significant decrease in intensity due to an antiferromagnetic coupling of the Cu^{2+} ions though the deprotonated pyrazolate bridge; the formation of a further hydroxo bridge between the metal ions (pH = 9) completely vanishes the signal. This is in agreement with previous reports in which Cu^{2+} ions were interconnected through 3,6-bis(2-pyridyl)pyridazine and hydroxo bridging ligands.[36,37]

The variations at pH = 6 in the visible spectra of **L1** and **L2** recorded upon addition of increasing amounts of Cu^{2+} denote some differential features for both systems (Fig. 7).

For **L1**, a d–d band centred at 560 nm is observed until a 1 : 1 molar ratio of Cu^{2+} : L is reached (ε = 115 L mol^{-1} cm^{-1}), then this band stops increasing in intensity and a new band bathochromically shifted at 716 nm appears that reaches its maximum intensity for 2 : 1 Cu^{2+} : **L1** molar ratio (ε = 140 L mol^{-1} cm^{-1}) (Fig. 7A).

In the case of **L2**, however, for Cu^{2+} : **L2** ratios below 1 a continuous increase of the band at 570 nm is observed that progressively shifts bathochromically to 600 nm increasing its intensity until a 2 : 1 molar ratio is reached (ε = 240 L mol^{-1} cm^{-1}) (Fig. 7B).

Interestingly, in the case of the largest ligand, **L3**, the addition of increasing amounts of Cu^{2+} at pH = 6 just leads to an increase in the absorbance of a band centred at 262 nm which reaches its maximum for 2 : 1 Cu^{2+}–**L3** without a significant shift in the wavelength of the band.

For a 1 : 1 Cu^{2+}–**L1** molar ratio, spectra recorded at pH values of 5, 8 and 11 where the mononuclear $[Cu\mathbf{HL1}]^{3+}$, $[Cu\mathbf{L1}]^{2+}$ and $[Cu\mathbf{L1}(OH)]^{+}$ species predominate, respectively, are practically the same with a d–d band centred at around 560 nm (ε = 130 L mol^{-1} cm^{-1}), only a small hypsochromic shift is observed for the last species (Fig. 8A).

While for pH values below 5 the spectra reveal characteristics of the mononuclear species with an absorption band at 560 nm, at pH 6.6 the $[Cu_2(H_{-1}\mathbf{L1})]^{3+}$ species predominates (Fig. 8B), in addition to the band at 560 nm, a new band centred at 710 nm (ε = 141 L mol^{-1} cm^{-1}) is observed. The formation of the hydroxylated species $[Cu_2(H_{-1}\mathbf{L1})(OH)]^{2+}$ and $[Cu_2(H_{-1}\mathbf{L1})(OH)_2]^{+}$, which predominate at pH values of 9 and 11 (Fig. 8B), leads to hypsochromic shifts of the less energetic band that now appears centred at *ca.* 650 nm (ε = 148 L mol^{-1} cm^{-1}; 134 mol^{-1} cm^{-1}). These spectral changes suggest a geometry change from essentially square planar for the mononuclear species as supported by the crystal structure **1** (*vide infra*) to a more pyramidal geometry[38] once the binuclear complex is formed following the deprotonation of the pyrazole moiety.

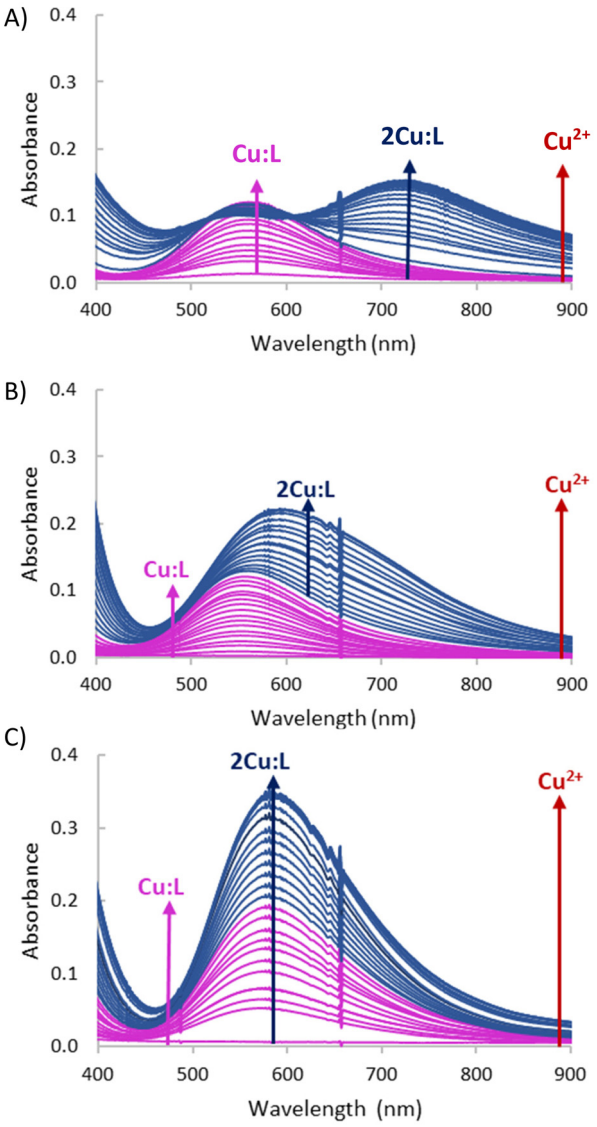

Fig. 7 Variation in the UV-Vis spectra of systems (A) Cu^{2+} : **L1**, (B) Cu^{2+} : **L2** and (C) Cu^{2+}–**L3** upon increasing additions of Cu^{2+} at pH = 6, the initial concentration of the ligands 1 × 10^{-3} M.

Crystal structure of $[Cu(HL1)Br]Br_{(1+x)}(ClO_4)_{(1-x)}{\cdot}yH_2O$ (1)

Crystals of **1** evolved by slow diffusion of acetone into an aqueous solution containing **L1**·6HBr, $Cu(ClO_4)_2{\cdot}6H_2O$ at pH 6. The crystals are composed of $[Cu(H_2(H_{-1}\mathbf{L1}))Br]^{2+}$ cations, bromide and perchlorate counter-anions and crystallization water molecules. Crystallographic data of the structures are provided in Table S3.†

The Cu^{2+} ion is coordinated with an almost square pyramidal geometry (Addison parameter λ = 0.03)[39] to one of the

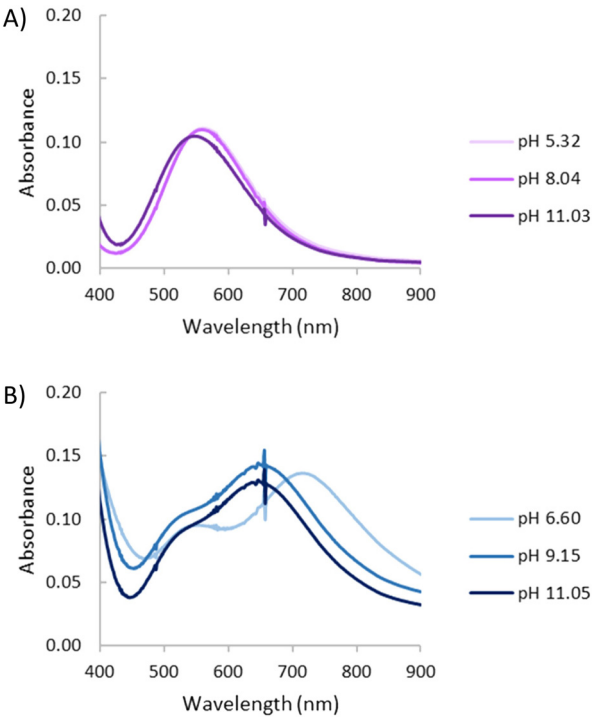

Fig. 8 UV-Vis spectra for the system Cu^{2+}–**L1** at variable pH. (A) $[Cu^{2+}] = [\mathbf{L1}] = 1 \times 10^{-3}$ M. (B) $[Cu^{2+}] = 2 \times 10^{-3}$ M, $[\mathbf{L1}] = 1 \times 10^{-3}$ M.

nitrogen donors of the pyrazole moiety, which acts as a monodentate ligand, and the three amine groups at the side of the coordinated pyrazole nitrogen donor that confirm the equatorial plane of the square pyramid (Fig. 9). As in previous cases, the shortest Cu^{2+}–N distance is the one with the pyrazole moiety.

The elevation of the Cu^{2+} atom over the plane defined by the equatorial donor atoms is 0.29 Å. The molecule is rather flat with the angle between the mean planes defined by the coordinated and non-coordinated donor atoms of 22°. A list of bond distances and angles is shown in Table 4. As previously mentioned, one point of interest regards the nature of the pyrazole ligand in the mononuclear complexes. The location of

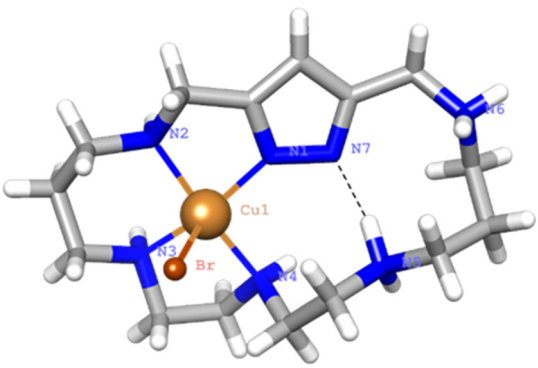

Fig. 9 View of the X-ray crystal structure of the complex cation $[Cu(H_2(H_{-1}\mathbf{L1}))Br]^{2+}$.

Table 4 Selected bond distances (Å) and angles (°) for **1**

Distances (Å)		Angles (°)	
Cu1–N1	1.985(2)	**N1–Cu1–N2**	81.9(1)
Cu1–N2	2.057(3)	**N2–Cu1–N3**	90.5(1)
Cu1–N3	2.021(3)	**N3–Cu1–N4**	84.9(1)
Cu1–N4	2.074(3)	**N1–Cu1–N4**	97.9(1)
Cu1–Br1	2.713(7)	**N1–Cu1–Br1**	102.69(7)
		N2–Cu1–Br1	96.61(7)
		N3–Cu1–Br1	94.21(8)
		N4–Cu1–Br1	99.21(7)

the residual electron density indicates that only about 22(5)% would remain in the pyrazole nitrogen and the other 78(5)% would be shifted towards amine N5 that, thereby, would gain a significant ammonium group characteristic. Therefore, in this case coordination of only one copper to the pyrazole polarizes the N–H bond facilitating its partly transfer to an amine group. The situation might be interpreted as if a strong intramolecular hydrogen bond between the ammonium and the pyrazolate would be formed (N–H···N 1.75(4) Å, 160(4)°). The uncoordinated side of the molecule is of interest since different guests could be bound taking advantage of coulombic interactions, hydrogen bonding and the assistance of the coordinated metal ion as a Lewis acid centre.

Also, it is interesting to remark that the coordination behaviour of this [1 + 1] pyrazole azacyclophane differs from that exhibited by related pyrazolaphanes with tetraamine bridges in which the formation of dimeric binuclear complexes was always observed. As commented before, the larger number of nitrogen atoms and greater flexibility of these ligands allow the convergence of an enough number of nitrogen atoms inwards facilitating the formation of monomeric complexes.

Crystal structure of $[Cu_2(H_{-1}\mathbf{L2})Cl(ClO_4)](ClO_4)\cdot H_2O\cdot C_2H_5OH$ (2)

Crystals of **2** were obtained by slow diffusion of ethanol into an aqueous solution of **L2**·6HCl and $Cu(ClO_4)_2\cdot 6H_2O$ at pH = 7. The asymmetric unit consists of $[Cu_2(H_{-1}\mathbf{L2})Cl(ClO_4)]^+$ cations, a perchlorate counter-anion and crystallisation water and ethanol molecules. The pyrazole moiety is deprotonated coordinating as a bis(monodentate) bridging ligand to the Cu^{2+} centres, which are placed at a distance of 4.213(3) Å (Fig. 10).

This distance is larger than those found in complexes where two pyrazolate moieties were simultaneously bridging the two Cu^{2+} metal ions. This was the case of monomeric complexes of either [2 + 2] pyrazole azamacrocycles[7,8] or dimeric complexes of [1 + 1] azamacrocycles.[14,15] In all these examples the Cu^{2+}–Cu^{2+} distance was about 4 Å. The copper atoms complete their coordination spheres with three consecutive amine groups at each side of the bridge and with either a chloride or a perchlorate anion that points towards different sides of the macrocyclic cavity. The coordination geometry for Cu1 is slightly distorted square pyramidal, and essentially regular square pyramidal for Cu2, with the chloride or perchlorate anions occupying the strongly elongated axial positions.

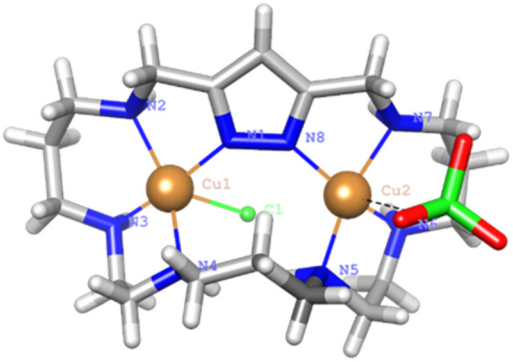

Fig. 10 View of the crystal structure of the binuclear cation complex $[Cu_2(H_{-1}\mathbf{L2})Cl(ClO_4)]^+$.

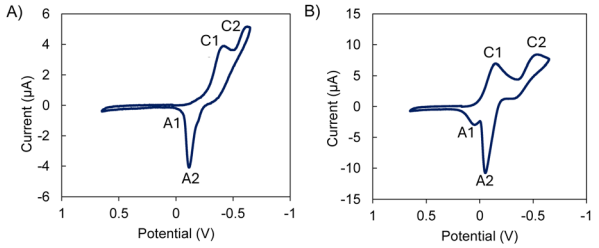

Fig. 11 Cyclic voltammograms at the glassy carbon electrode for aqueous solution of the mononuclear (A) Cu–**L1** and the binuclear (B) Cu_2**L1** systems, 1×10^{-4} M, in 0.15 M NaCl at pH 7.0. Scan rate 50 mV s^{-1}.

Addison parameters are λ = 0.23 and λ = 0.05, respectively.[39] The shortest Cu–N distances are those established with the nitrogen atoms of the pyrazole rings. The distances and angles of the coordination sites are reported in Table 5.

The elevation of the metal ion with respect to the mean equatorial plane defined by the coordinated nitrogen atoms is 0.23 Å for Cu1 while Cu2 is completely embedded in the plane. The angle between the equatorial planes of both sites is 64°. In the tridimensional arrangement the binuclear complexes are organised in couples interconnected by a hydrogen bond network involving the chloride anion bound to Cu1, the ethanol molecules and two of the coordinated amine groups to Cu1 (N2–H2, N3–H3) (see Fig. 10).

Electrochemistry

The reduction potential is one of the most important chemical properties when designing superoxide dismutase mimetics, as at physiological pH it must be less negative than the reduction potential for the oxygen/superoxide anion couple (E^0 O_2/O_2^- = −0.33 V *vs.* NHE) but less positive than the superoxide anion/water couple (E^0 O_2^-/H_2O = +0.89 V *vs.* NHE).[40] The voltammetric response of the studied complexes was highly homogeneous. As shown in Fig. 11 and Fig. S33,† the cyclic voltammograms consist of two more or less overlapped cathodic peaks at *ca.* −0.40 (C1) and −0.75 V (C2) *vs.* Ag/AgCl. In the subsequent anodic scan, a typical stripping peak was recorded at −0.10 V (A2) followed by a second weak oxidation wave at potentials between −0.05 and +0.18 V (A1) depending on the studied complex. Experiments performed in different potential ranges revealed that the process A2 is coupled with the previous signal C2. This denotes that this cathodic process leads to the formation of copper metal. In turn, the signal C1 can be attributed to the Cu^{2+} reduction to Cu^+. This signal often appears as a separate peak (**L1**) or as a shoulder (**L2**, **L3**) preceding the cathodic peak C2.

This suggests that there is no direct $Cu^{II}L \rightarrow Cu^{I}L \rightarrow Cu^0$ + L reduction *via* two successive one-electron reductions. The peak A1 appears at potentials at which the oxidation of Cu^+–chloride complexes to the corresponding Cu^{2+}-chloride complexes occurs. Given the high concentration of NaCl in the supporting electrolyte solution, it is conceivable that these signals reflect the formation of Cu^+–chloride complexes when the deposit of metallic copper generated in the cathodic process C2 is oxidized in the oxidative dissolution process A2. Interestingly, the peak current per mole of copper of process C2 is the same (within the range of experimental uncertainty) for all four tested complexes. This feature suggests that in the case of the binuclear complexes, both metal centres are reduced simultaneously and independently.

This voltammetry can be interpreted in terms of the coexistence of two reductive pathways, the first one involving the one electron reduction of the parent $Cu^{II}L$ and Cu^{II}_2L complexes to analogue $Cu^{I}L$ and Cu^{I}_2L ones (C1 peak). As judged from previous studies on Cu–receptor complexes,[19,41–43] the progress from the process C1 to the process C2 involves some previous coordinative rearrangement of the Cu^{I} intermediate. Alternatively, this species can undergo disproportionation so that the peak C2 is equivalent to the two-electron reduction of the $Cu^{II}L$ and Cu^{II}_2L complexes to Cu metal. The apparent formal electrode potential of the Cu^{II}/Cu^{I} couple was calculated as the half peak potential of the signal C1. The calculated apparent formal electrode potentials are representative of the potential SOD activity of the complexes. These values remain intermediate between −0.33 V and +0.89 V *vs.* NHE as desired, but presenting significant variations between the different species, being more positive for the binuclear complexes (+0.10 V for Cu_2**L1** and −0.05 V *vs.* NHE for Cu_2**L2** and Cu_2**L3**) than for the corresponding mononuclear species (−0.10 V for Cu**L1** and −0.15 V *vs.* NHE for Cu**L2** and Cu**L3**).

Table 5 Selected bond distances (Å) and angles (°) for **2**

Distances (Å)		Angles (°)			
Cu1–N1	1.972(9)	**N1–Cu1–N2**	80.8(4)	**N1–Cu1–Cl1**	84.8(3)
Cu1–N2	2.081(9)	**N2–Cu1–N3**	92.9(4)	**N2–Cu1–Cl1**	117.0(3)
Cu1–N3	1.998(9)	**N3–Cu1–N4**	85.2(4)	**N3–Cu1–Cl1**	89.1(3)
Cu1–N4	2.11(1)	**N1–Cu1–N4**	104.9(4)	**N4–Cu1–Cl1**	89.1(3)
Cu1–Cl1	2.741(3)				
Cu2–N5	2.00(1)	**N5–Cu2–N6**	87.1(6)	**N5–Cu2–O22**	84.0(5)
Cu2–N6	2.02(1)	**N6–Cu2–N7**	88.9(7)	**N6–Cu2–O22**	90.8(6)
Cu2–N7	2.04(1)	**N7–Cu2–N8**	82.5(6)	**N7–Cu2–O22**	78.4(6)
Cu2–N8	1.97(1)	**N5–Cu2–N8**	107.3(5)	**N8–Cu2–O22**	108.3(5)
Cu2–O22	2.65(2)				

Evaluation of the superoxide dismutase activity

In view of the interesting SOD activity of the analogous complexes of the ligands **L4** and **L5** containing pyridine instead of 1*H*-pyrazole rings, and taking into account the ability of the uncoordinated pyrazole nitrogen to form hydrogen bonds (*vide supra*), we made preliminary assays about the potentiality of the Cu^{2+} complexes of **L1–L3** to behave as SOD mimics. SOD activity was evaluated at physiological pH by means of the indirect enzymatic assay McCord–Fridovich,[44] which allows calculating the IC_{50} and catalytic constant (k_{cat}) values for both the mononuclear and binuclear Cu^{2+} complexes of **L1**, **L2** and **L3** as well as for the free **L1**, **L2** and **L3** macrocycles. Table 6 shows these values along with the previously reported ones for the Cu^{2+}–**L3** and Cu^{2+}–**L4** pyridine-based analogous binuclear systems,[19] and for the native CuZn-SOD enzyme and the free Cu^{2+} ion in aqueous solution.

As we can see in Table 6, both the mononuclear and binuclear Cu^{2+}–**L1**, Cu^{2+}–**L2** and Cu^{2+}–**L3** systems exhibit SOD activity. However, in all three systems the binuclear complexes show clearly higher antioxidant activity than the mononuclear ones. The non-saturated coordination spheres of the metal ions in the binuclear complexes and the close proximity between the metal ions should likely contribute to the enhanced activity of these complexes. Furthermore, the activity found for the binuclear systems of **L2** and **L3** is very remarkable with IC_{50} and k_{cat} values close to those reported for the native enzyme, constituting two of the as far as we know best results reported in the literature. In order to facilitate the discussion of the results, Fig. 12 plots the k_{cat} values for the mononuclear and binuclear Cu^{2+}–**L1**, Cu^{2+}–**L2** and Cu^{2+}–**L3** systems, as well as those of the binuclear complexes of the pyridinaphanes **L4** and **L5**. Interestingly, the replacement of the pyridine moiety by the pyrazole one leads to a slight enhancement in the SOD activity of the systems.

One plausible explanation might be the presence of the N–H in the 1*H*-pyrazole moiety, which might be involved in hydrogen bonding with the incoming superoxide anion. On the other hand, the imidazole of the His-61 residue in the native CuZn-SOD enzyme seems to play a key role during the catalytic pathway, allowing the formation and breaking of an imidazolate bridge.[21,22]

Table 6 IC_{50} and k_{cat} values for the Cu^{2+}–**L1**, Cu^{2+}–**L2** and Cu^{2+}–**L3** systems and for the free **L1**, **L2** and **L3** ligands obtained by the McCord–Fridovich method, along with some examples reported in the literature

System	IC_{50} (μM)	k_{cat} (10^6 M^{-1} s^{-1})	Ref.
Cu**L1**	1.72(1)	2.7	
Cu_2**L1**	0.6(1)	7.9	
Cu**L2**	7.34(4)	0.4	
Cu_2**L2**	0.06(1)	53.0	
Cu**L3**	5.90(34)	0.5	
Cu_2**L3**	0.03(1)	104.0	
Cu_2**L4**	0.22 (4)	13.5	19
Cu_2**L5**	0.11 (2)	27.9	19
CuZn-SOD	0.010(2)	430.0	19
$Cu(ClO_4)_2$	1.1(1)	2.7	19

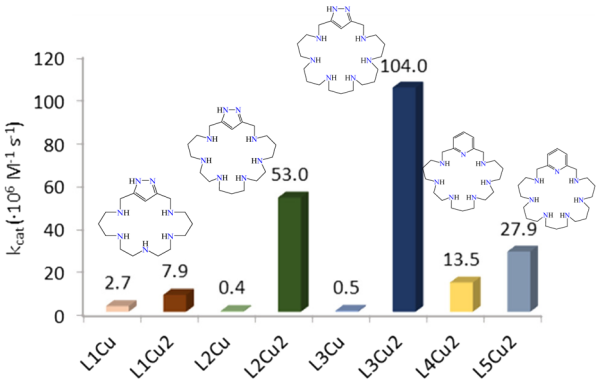

Fig. 12 Plot of the k_{cat} values for the mononuclear and binuclear Cu^{2+}–**L1**, Cu^{2+}–**L2**, Cu^{2+}–**L3**, Cu^{2+}–**L4** and Cu^{2+}–**L5** systems.

Finally, preliminary studies on hydrogen peroxide removal performed using the xylenol orange method[45] show moderate capacity of the binuclear complexes. A more thorough analysis of the ROS scavenging capacity of these systems is currently under study.

Conclusions

The studies presented here show that the polyamine length and the number of nitrogen atoms of the bridges in pyrazolaazacyclophanes regulate the endo- or exo-coordinate binding modes of the bis(monodentate) pyrazolate moiety. While shorter tetraamine bridges give rise to exo-coordination with the formation of dimeric species of 2 : 1, 3 : 2 or 4 : 2 Cu^{2+} : L stoichiometry, longer pentaamine or hexaamine bridges lead to the formation of discrete monomeric binuclear complexes. In these complexes a single pyrazolate bridge connects the metal ions which complete their coordination spheres with the nitrogen atoms of the bridges and, if necessary, with exogenous ligands. This has been proven both in solution by a variety of experimental techniques and by solid state by X-ray diffraction analysis. The presence of a single pyrazolate bis (monodentate) bridge places the metal ions at distances close to those shown by copper enzymes participating in ROS removal, at the time that leave enough room to allow the binding of the substrates to the metal centre. This situation has produced two of the potential SOD mimics with the highest activity so far reported in the literature with IC_{50} values approaching those displayed by the native enzymes. Further studies on the biological capacity of these complexes and derivatives are currently underway.

Experimental section

The synthesis of **L2** and **L3** was performed as described in ref. 16. The compounds gave satisfactory elemental microanalysis and spectroscopic characterization results. 1*H*-3,5-Bis(chloromethyl)pyrazole and 3,5-bis-(chloromethyl)-1-(tetrahydropyran-

2-yl)-pyrazole were prepared as described in the literature.[26,46] The tosylated amine 1,5,8,11,15-penta(*p*-tosylsulfonyl)-pentaazapentadecane was prepared as described in ref. 47.

Synthesis of 11-tetrahydropyran-2-yl-3,7,10,13,17-pentaaza-3,7,10,13,17-*p*-toluensulfonyl-1-(3,5)-pyrazolacyclooctadecaphane. The tosylated amine 1,5,8,11,15-penta(*p*-tosylsulfonyl)-pentaazapentadecane (5.0 mmol) and K_2CO_3 (50.0 mmol) were suspended in 250 mL of anhydrous acetonitrile in a round-bottom flask. 3,5-Bis-(chloromethyl)-1-(tetrahydropyrane-2-yl)-pyrazole (5.0 mmol) was dissolved in 150 mL of anhydrous acetonitrile and dropwise added over one hour. The suspension was refluxed for 48 h under a nitrogen atmosphere, and then filtered off. The solution was vacuum evaporated to dryness. Purification was carried out by column chromatography (silica gel, dichloromethane/acetone 25/1) to give the product as a white solid. Yield: 64%. ^{1}H NMR (300 MHz, $CDCl_3$) δ 7.72–7.63 (m, 10H), 7.37–7.27 (m, 10H), 6.18 (s, 1H), 5.56 (d, J = 8.2 Hz, 1H), 4.56 (d, J = 14.9 Hz, 1H), 4.36 (d, J = 15.2 Hz, 1H), 4.06 (dd, J = 23.7, 15.1 Hz, 2H), 3.93 (m, 1H), 3.74 (m, 1H), 3.36–2.84 (m, 1H), 2.47–2.39 (m, 17H), 2.24 (m, 15H), 1.90 (m, 1H), 1.76–1.56 (m, 8H). ^{13}C NMR (300 MHz, $CDCl_3$): δ 149.70, 143.70, 144.10, 138.10, 139.80, 128.90, 105.50, 100.10, 68.10, 50.10, 49.10, 48.70, 47.90, 29.90, 24.40, 25.30, 23.30, 21.30.

Synthesis of 3,7,10,13,17-pentaaza-1-(3,5)-pyrazolacyclooctadecaphane (L1·6HBr·2H$_2$O). The protected macrocycle (2.0 mmol) and phenol (12 equivalents per protective group) were suspended in HBr-AcOH 33% (12 L per protective group). The mixture was stirred at 90 °C for 14 h and then was cooled. The resulting residue was filtered off and washed with acetone to give **L1** as its hydrobromide salt. Yield: 75%. ^{1}H NMR (300 MHz, D_2O) δ 6.85 (s, 1H), 4.42 (s, 4H), 3.57 (s, 8H), 3.42–3.25 (m, 8H), 2.27–2.15 (m, 4H). ^{13}C NMR (75 MHz, D_2O) δ 141.06, 112.25, 47.16, 46.35, 46.14, 44.98, 25.32. ESI–MS (m/z): calculated for $[L + H]^+$: 310.5. Found: 310.3. Elemental analysis: calculated for $C_{15}H_{31}N_7$·6HBr·2H_2O: N, 19.25; H, 7.42; C, 32.45. Found: N, 19.19; H, 6.75; C, 32.85.

Electromotive force measurements. The potentiometric titrations were carried out at 298.1 ± 0.1 K using NaCl 0.15 M as the supporting electrolyte. The experimental procedure (burette, potentiometer, cell, stirrer, microcomputer, *etc.*) has been fully described elsewhere.[48] The acquisition of the *emf* data was performed with the computer program PASAT[49] The reference electrode was a Crison 52 40 Ag/AgCl electrode in 0.5 M NaCl solution. A Wilhelm bridge filled with 0.5 M NaCl was used to separate the glass and reference electrodes. The glass electrode (Crison 52 50 Ag/AgCl) was calibrated as an hydrogen-ion concentration probe by titration of previously standardized amounts of HCl with CO_2-free NaOH solutions and determining the equivalent point by Gran's method,[50,51] which gives the standard potential, $E'°$, and the ionic product of water (pK_w = 13.73(1)). The computer program HYPERQUAD[28] was used to fit the protonation and stability constants. Solutions containing the ligand salts with Cu^{2+} : L molar ratios varying from 2 : 1 to 1 : 2 were titrated with NaOH with Cu^{2+} concentrations ranging from 2.0 × 10^{-4} M to 1.1 × 10^{-3} M. The different titration curves for each system were treated as separated curves without significant variations in the values of the stability constants. Finally, the sets of data were merged together and treated simultaneously to give the final stability constants. When more than one model fits the experimental data, the most reliable chemical model was chosen by performing F tests at the 0.05 confidence level.[52,53]

NMR measurements. The ^{1}H and ^{13}C NMR spectra were recorded on a Bruker Advance DPX 300 MHz and a Bruker Advance DPX 400 MHz spectrometer operating at 299.95 MHz and 399.95 MHz for ^{1}H NMR and at 75.43 MHz and 100.58 MHz for ^{13}C NMR. *tert*-Butyl alcohol was used as a reference standard (δ = 1.24 ppm for ^{1}H and δ = 70.36 ppm for ^{13}C).[54] Adjustments to the desired pH were made using drops of DCl and/or NaOD solutions. The pD was calculated from the measured pH values using the correlation, pH = pD − 0.4.[55]

X-ray analysis. The crystals were measured on a Bruker D8 Venture X-ray diffractometer using MoKα radiation (λ = 0.71073 Å) equipped with an Oxford low temperature unit operating at 120 K. Indexing, strategy and data collection were performed with APEX3 software suite. OLEX2 [56] was used as front-end for solving and refining. The initial structure was solved with direct methods using SHELXS and then refined with SHELXL2018.[57] Initially, an isotropic refinement was performed on the non-hydrogen atoms. Then, anisotropic refinement was done.

Computational studies. The modelling of the Cu^{2+} complexes was performed using the density functional theory computational method as well as the Becke three-parameter Lee–Yang–Parr hybrid functional (B3LYP).[58–60] All the gas-phase optimizations were carried out by using the Ahlrichs' basis set def2-TZV(P)[61] for all atoms except for copper, for which we employed the MDF10 Stuttgart–Dresden effective core potential.[62] The influence of dispersion was also taken into account by means of Grimme's dispersion (IOp(3/124 = 30)) correction, while the effect of the polarizable solvent (water) was considered by using the default SCRF method of the Polarizable Continuum Model.[63,64] Vibrational frequencies were computed for each minimum energy structure and, for each one of them, the zero-point correction was also calculated and applied. Computations were carried out using the program Gaussian09 C.01.[65] gMolden[66] and PyMOL[67] were used for visual inspection and to create the molecular graphics.

Mass spectrometry. HR-ESI mass spectra of solutions (water/methanol 50/50 vol/vol) containing a given ligand and Cu$(ClO_4)_2$·6H_2O in 1 : 1 and 2 : 3 molar ratios were acquired in the positive ion mode using a Triple TOF 5600 hybrid quadrupole time-of-flight (TOF) mass spectrometer. N_2 was used as a curtain and nebulizing gas. The experiments were performed at a voltage of 5300 V and GS1 and GS2 (35 psi) ion source gas at 723.15 K. The AB SCIEX Peak View software was used for the analysis of the data.

UV-vis spectroscopy. UV-vis spectra of the samples containing Cu^{2+} and the ligand s in 1 : 1 and 2 : 1 molar ratios (1.0 ×

10^{-3} M) were recorded with an Agilent 8453 spectrometer at 298.15 K.

Electron paramagnetic resonance spectroscopy. X-band EPR spectra (ν = 9.47 GHz) of the frozen-matrix aqueous solutions at 70 K and Q-band EPR spectra (ν = 34.03 GHz) of Cu^{2+} : **L2** at 1 : 1 molar ratio were recorded under non-saturating conditions on a Bruker ER 200 D spectrometer equipped with a helium cryostat.

Paramagnetic NMR spectroscopy. The paramagnetic NMR measurements were acquired on a Bruker Avance400 spectrometer operating at 399.91 MHz. One-dimensional spectra were recorded in D_2O solvent with presaturation of the H_2O signal during part of the relaxation delay to eliminate the H_2O signal. Relaxation delay times of 100–400 ms, spectral widths in the range of 40–80 KHz and acquisition times of 60–300 ms were used. 1D spectra were processed using exponential line-broadening weighting functions as apodization with values of 20–30 Hz. Chemical shifts were referenced to residual solvent protons of D_2O resonating at 4.76 ppm (298 K) relative to TMS. Sample concentrations of the complexes for paramagnetic ^{1}H NMR were 5 mmol dm^{-3} for Cu_2(**L1**) and 10 mmol dm^{-3} for Cu_2(**L3**). Transversal relaxation times were obtained measuring the line broadening of the isotropically shifted signals at half-height through the equation $T_2^{-1} = \pi\Delta\nu_{1/2}$.

Electrochemical measurements. Cyclic voltammetry experiments were performed on $Cu(ClO_4)_2{\cdot}6H_2O$ plus ligand solutions in 0.10 M Tris buffer at pH 7.4. Electrochemical experiments were performed with a CH 440I potentiostat in a conventional three-electrode cell using a glassy-carbon working electrode (BS MF2012, geometrical area 0.071 cm^2) previously cleaned and activated with an aqueous suspension of alumina on a soft surface, dried and cleaned. An AgCl (3 M NaCl)/Ag and a platinum-wire auxiliary electrode completed the three-electrode arrangement. The cyclic voltammograms were recorded at scan rates of 10–2000 mV s^{-1} in solutions optionally deaerated by bubbling Ar for 10–15 min.

Superoxide dismutase assay. The SOD-like activity was determined by using the nitro blue tetrazolium (NBT) method.[44] The assays were carried out in a pH = 7.4 50 mM HEPES buffer at 298.1 K. The xanthine (2.2×10^{-4} M)/xanthine oxidase system was used to generate a reproducible and constant flux of superoxide anions. The rate of reduction of NBT (7.3×10^{-5} M) to blue formazan was followed spectrophotometrically at 560 nm. Data in the absence of the complex were used as a reference. The rate of NBT reduction was inhibited after the addition of the complex solutions at increasing concentrations prepared in 50 mM Tris-HCl buffer. The percentage of inhibition of the NBT reduction was used as a measure of the SOD activity of the compounds. The concentration of the complex required to yield 50% inhibition of NBT reduction (IC_{50}) was determined from a plot of percentage inhibition *versus* complex concentration. The IC_{50} data have been calculated from the mean values of at least three independent measurements. The catalytic constant was calculated from the IC_{50} using the equation $k_{cat} = k_{NBT}[NBT]/IC_{50}$ where $k_{NBT} = (5.9 \pm 0.5) \times 10^5$ M^{-1} s^{-1}.[68] Blank experiments were recorded with the ligands and/or the nanoparticles alone without observing any effect. Moreover, kinetics with the BNP + Cu^{2+} system were also determined in the absence of the ligands, and no significant difference in the catalytic activity of solutions of free Cu^{2+} without BNP was observed.

Data availability

Crystallographic data for compounds **1** and **2** have been deposited at the CCDC repository under the accession numbers 2240668 and 2215780.†

^{1}H and ^{13}C NMR spectra of compounds **L1**, **L2** and **L3**, mass spectra of the Cu^{2+} complexes, distribution diagrams of the free ligands and metal complexes, and protonation and stability constants are included as a part of the ESI.†

Author contributions

I. Bonastre-Sabater: investigation, writing – original draft, and writing – review & editing; A. Lopera: investigation; A. Martínez-Camarena: formal analysis and writing – original draft; Salvador Blasco: formal analysis; A. Doménech-Carbó: formal analysis, writing – original draft, and writing – review & editing; H. R. Jimenez: investigation, writing – original draft and writing – review & editing; B. Verdejo: investigation and writing – review & editing; E. García-España: conceptualization, formal analysis, funding acquisition, methodology, project administration, supervision, validation, and writing – review & editing; M. P. Clares: conceptualization, project administration, supervision, validation, and writing – review & editing.

Conflicts of interest

There are no conflicts to declare.

Acknowledgements

Financial support from the Spanish Ministerio de Economía y Competitividad (Project PID2019-110751RD-I00) and the Conselleria de Innovación, Universidades, Ciencia y Sociedad Digital of the Generalitat Valenciana (PROMETEO Grant CIPROM/2021/030) is acknowledged. A. M.-C. wants to acknowledge the support received under the "Margarita Salas" post-doctoral program (grant MS21-095) funded by the Ministerio de Universidades from the Spanish Government and the European Union – NextGenerationEU.

References

1 (*a*) J. Elguero, in *Pyrazoles in Comprehensive Heterocycle Chemistry II; A Review of the Literature 1982–1995*, ed. A. R. Katrizky, C. V. Ress and E. F. V. Scriven, Pergamon

New York, 1997, vol. 3, pp. 1–75; (*b*) R. Muckheerjee, *Coord. Chem. Rev.*, 2000, **203**, 151–258.

2 (*a*) J. Bedi, V. Muelas-Ramos, M. Peñas-Garzón, A. Gómez-Avilés, J. J. Rodríguez and C. Belver, *Catalysts*, 2019, **9**, 52; (*b*) Y. Li, R. Wang, X. Liu, K. Li and Q. Xu, *Nanotechnology*, 2023, **34**, 202002; (*c*) K. Wang, X.-L. G Lv, D. Feng, J. Li, S. Chen, J. Sun, L. Song, Y. Xie, J.-R. Li and H.-C. Zhou, *J. Am. Chem. Soc.*, 2016, **138**, 914–919; (*d*) S. Saha, M. Das, K. S. Das, R. Datta, S. Bala, J.-L. Liu, P. P. Ray and R. Mondal, *Cryst. Growth Des.*, 2023, **23**, 1104–1118; (*e*) S. Posada-Pérez, J. Poater, N. Bahri-Laleh and A. Poater, *Catalysts*, 2023, **13**, 317; (*f*) M. El Boutaybi, A. Taleb, R. Touzani and Z. Bahari, *Mater. Today: Proc.*, 2020, **31**, S96–S102.

3 (*a*) R. K. Gupta, P. Kallem, G. G. Luo, P. Cui, Z. Wang, F. Banat, C.-H. Tung and D. Sun, *Chem. Rev.*, 2023, **497**, 215436; (*b*) A. Lancheros, S. Goswami, M. R. Mian, X. Zhang, X. Zarate, E. Schott, O. K. Farha and J. T. Hupp, *Dalton Trans.*, 2021, **50**, 2880–2890.

4 (*a*) S. Hamood, S. Azzam and M. A. Pasha, *European J. Pharm. Med. Res.*, 2020, **7**, 867–887; (*b*) L. M. R. Orlando, G. C. Lechuga, L. S. Lara, B. S. Ferreira, C. N. Pereira, R. C. Silva, M. S. Santo and M. C. S. Pereira, *Molecules*, 2021, **26**, 6742; (*c*) S. Kumari, S. Paliwal and R. Chauhan, *Synth. Commun.*, 2014, **44**, 1521–1578.

5 (*a*) R. H. Holm, P. Kennepohl and E. I. Solmon, *Chem. Soc. Rev.*, 1996, **96**, 2239–2314; (*b*) E. I. Solomon, U. M. Sundaram and T. E. Machonkin, *Chem. Rev.*, 1996, **98**, 2563–2605; (*c*) S. Ferguson-Miller and G. T. Babcock, *Chem. Rev.*, 1996, **96**, 2889–2907; (*d*) H. Decker, T. Schweikardt and F. Tuczek, *Angew. Chem., Int. Ed.*, 2006, **45**, 4546–4550; (*e*) N. Kitajima, K. Fujisawa, C. Fujimoto, Y. Morooka, S. Hashimoto, T. Kitagawa, K. Toriumi, K. Tatsumi and A. Nakamura, *J. Am. Chem. Soc.*, 1992, **114**, 1277–1291; (*f*) Y. Sheng, I. A. Abreu, D. E. Cabelli, M. J. Maroney, A.-F. Miller, M. Teixeira and J. S. Valentine, *Chem. Rev.*, 2014, **114**, 3854–3918.

6 (*a*) P. Chaudhuri, V. Kataev, B. Düchner, H. Kaluss, B. Kersting and F. Meyer, *Coord. Chem. Rev.*, 2009, **253**, 2261–2283; (*b*) J. L. Vlugt, S. Demeshko, S. Dechert and F. Meyer, *Inorg. Chem.*, 2008, **47**, 1576–1585; (*c*) A. Prokofieva, A. Prikhodko, E. Enyedy, E. Farkas, W. Maringele, S. Demeshko, S. Dechert and F. Meyer, *Inorg. Chem.*, 2007, **46**, 4298–4307; (*d*) A. Eisenwiener, M. Neuberger and T. Kaden, *Dalton Trans.*, 2007, 218–223; (*e*) S. Brooker, T. C. Davidson, S. J. Hay, R. J. Kelly, D. K. Kennepohl, P. G. Plieger, B. Moubaraki, K. S. Murray, E. Bill and E. Bothe, *Coord. Chem. Rev.*, 2001, **216–217**, 3–30; (*f*) H. Weller, L. Siegfred, M. Neugerger, M. Zhender and T. A. Kaden, *Helv. Chim. Acta*, 1997, **80**, 2315–2328; (*g*) A. Eisenwiener, M. Neuberger and T. A. Kaden, *Dalton Trans.*, 2007, 218–223.

7 (*a*) M. Kumar, V. J. Arán and P. Navarro, *Tetrahedron Lett.*, 1993, **34**, 3159–3162; (*b*) V. J. Arán, M. Kumar, J. Molina, L. Lamarque, P. Navarro, E. García-España, J. A. Ramírez, S. V. Luis and B. Escuder, *J. Org. Chem.*, 1999, **64**, 6135–6146; (*c*) C. Miranda, F. Escartí, L. Lamarque, E. García-España, P. Navarro, J. Latorre, F. Lloret, H. R. Jiménez and M. J. R. Yunta, *Eur. J. Inorg. Chem.*, 2005, 189–208; (*d*) C. Miranda, F. Escartí, L. Lamraque, M. J. R. Yunta, P. Navarro, E. Gracía-España and M. L. Jimeno, *J. Am. Chem. Soc.*, 2004, **126**, 823–833; (*e*) J. Pitarch, M. P. Clares, R. Belda, R. D. Costa, P. Navarro, E. Ortí, C. Soriano and E. García-España, *Dalton Trans.*, 2010, **39**, 7741–7746.

8 (*a*) M. Kumar, V. J. Arán and P. Navarro, *Tetrahedron Lett.*, 1995, **12**, 2161–2164; (*b*) L. Lamarque, C. Miranda, P. Navarro, F. Escartí, E. García-España, J. Latorre and J. A. Ramírez, *Chem. Commun.*, 2000, 1337–1338; (*c*) L. Lamarque, P. Navarro, C. Miranda, V. J. Arán, C. Ochoa, F. Escartí, E. García-España, J. Latorre, S. V. Luis and J. F. Miravet, *J. Am. Chem. Soc.*, 2001, **123**, 10560–10570.

9 J. Pitarch-Jarque, R. Belda, S. Blasco, P. Navarro, R. Tejero, J. M. Junquera-Hernández, V. Pérez-Mondéjar and E. García-España, *New J. Chem.*, 2016, **40**, 5670–5674.

10 (*a*) F. Escartí, C. Miranda, L. Lamarque, J. Latorre, E. García-España, M. Kumar, V. J. Arán and P. Navarro, *Chem. Commun.*, 2002, 936–937; (*b*) J. Pitarch-Jarque, K. Rissanen, S. García-Granda, A. Lopera, M. P. Clares, E. García-España and S. Blasco, *New J. Chem.*, 2019, **43**, 18915–18924.

11 J. Pitarch-Jarque, R. Belda, F. Lloret, J. Ferrando-Soria, P. Navarro, A. Lopera and E. García-España, *Dalton Trans.*, 2015, **44**, 3378–3383.

12 J. Pitarch-Jarque, R. Belda, L. García-España, J. M. Llinares, F. F. Pen, K. Rissanen, P. Navarro and E. García-España, *Dalton Trans.*, 2015, **44**, 7761–7764.

13 M. I. Rodríguez-Franco, P. San Lorenzo, A. Martínez and P. Navarro, *Tetrahedron*, 1999, **55**, 2763–2772.

14 R. Belda, J. Pitarch-Jarque, C. Soriano, J. M. Llinares, S. Blasco, J. Ferrando-Soria and E. García-España, *Inorg. Chem.*, 2013, **52**, 10795–10803.

15 A. Lopera, A. Gil-Martínez, J. Pitarch-Jarque, B. Verdejo, S. Blasco, M. P. Clares, H. R. Jiménez and E. García-España, *Dalton Trans.*, 2020, **49**, 8614–8624.

16 A. Lopera, J. A. Aguilar, R. Belda, B. Verdejo, J. W. Steed and E. García-España, *Soft Matter*, 2020, **16**, 6514–6522.

17 P. J. Altman and A. Pothig, *J. Am. Chem. Soc.*, 2018, **138**, 13171–13174.

18 (*a*) M. P. Clares, S. Blasco, M. Inclán, L. del Castillo Agudo, B. Verdejo, C. Soriano, A. Doménech, J. Latorre and E. García-España, *Chem. Commun.*, 2011, **47**, 5988–5990; (*b*) M. P. Clares, C. Serena, S. Blasco, A. Nebot, L. del Castillo, C. Soriano, A. Domènech, A. V. Sánchez-Sánchez, L. Soler-Calero, J. L. Mullor, A. García-España and E. García-España, *J. Inorg. Biochem.*, 2015, **143**, 1–8; (*c*) C. Serena, E. Calvo, M. P. Clares, M. L. Diaz, J. U. Chicote, R. Beltrán-Debon, R. Fontova, A. Rodriguez, E. García-España and A. García-España, *PLoS One*, 2015, **10**, 1–12; (*d*) M. Merino, M. D. Sequedo, A. V. Sánchez-Sánchez, M. P. Clares, E. García-España, R. P. Vázquez-Manrique and J. L. Mullor, *Int. J. Mol. Sci.*, 2022, **23**, 8936;

(*e*) M. Merino, S. González, M. C. Tronch, A. V. Sánchez-Sánchez, M. P. Clares, A. García-España, E. García-España and J. L. Mullor, *Int. J. Mol. Sci.*, 2023, **24**, 15153.

19 R. Belda, S. Blasco, B. Verdejo, H. R. Jiménez, A. Doménech-Carbó, C. Soriano, J. Latorre, C. Terencio and E. García-España, *Dalton Trans.*, 2013, **42**, 11194–11204.

20 (*a*) A. Martínez-Camarena, E. Delgado-Pinar, C. Soriano, J. Alarcón, J. M. Llinares, R. Tejero and E. García-España, *Chem. Commun.*, 2018, **54**, 3871–3874; (*b*) A. Martínez-Camarena, J. M. Llinares, A. Domènech-Carbó, J. Alarcón and E. García-España, *RSC Adv.*, 2019, **9**, 41549–41560.

21 (*a*) R. Sandhir, A. Yadav, A. Sunkaria and N. Singhal, *Neurochem. Int.*, 2015, **89**, 209–226; (*b*) H. Zhao, R. Zhang, X. Yan and K. Fan, *J. Mater. Chem. B*, 2021, **9**, 6939–6957.

22 (*a*) K. M. Lincoln, T. E. Richardson, L. Rutter, P. González, J. Simpkins and K. N. Green, *ACS Chem. Neurosci.*, 2012, **3**, 919–927; (*b*) K. M. Lincoln, P. González, T. E. Richardson, D. A. Julovich, R. Saunders, J. W. Simpkins and K. N. Green, *Chem. Commun.*, 2013, **49**, 2712–2714; (*c*) K. Lincoln, M. E. Offutt, T. D. Hayden, R. E. Saunders and K. N. Green, *Inorg. Chem.*, 2014, **53**, 1406–1416.

23 A. Martínez-Camarena, M. Merino, A. V. Sánchez-Sánchez, S. Blasco, J. M. Llinares, J. L. Mullor and E. García-España, *Chem. Commun.*, 2022, **58**, 5021–5024.

24 A. Martínez-Camarena, P. A. Sánchez-Murcia, S. Blasco, L. González and E. García-España, *Chem. Commun.*, 2020, **56**, 7511–7514.

25 (*a*) J. E. Richman and T. J. Atkins, *J. Am. Chem. Soc.*, 1974, **96**, 2268–2270; (*b*) A. Bencini, M. I. Burguete, E. García-España, S. V. Luis, J. F. Miravet and C. Soriano, *J. Org. Chem.*, 1993, **58**, 4749.

26 J. C. Röder, F. Meyer and H. Pritzkow, *Organometallics*, 2001, **20**, 811–817.

27 P. Gans, A. Sabatini and A. Vacca, *Talanta*, 1996, **43**, 1739.

28 L. Alderighi, P. Gans, A. Ienco, D. Peters, A. Sabatini and A. Vacca, *Coord. Chem. Rev.*, 1999, **184**, 311–318.

29 G. Yagil, *Tetrahedron*, 1967, **23**, 2855–2861.

30 J. Catalán, R. M. Claramunt, J. Elguero, J. Laynez, M. Menéndez, F. Anvia, J. H. Quian, M. Taagepera and R. W. Taft, *J. Am. Chem. Soc.*, 1988, **110**, 4105–4111.

31 (*a*) A. Bencini, A. Bianchi, E. García-España, M. Micheloni and J. A. Ramírez, *Coord. Chem. Rev.*, 1999, **188**, 97–156; (*b*) A. Bianchi, B. Escuder, E. García-España, S. V. Luis, V. Marcelino, J. F. Miravet and J. A. Ramírez, *J. Chem. Soc., Perkin Trans. 2*, 1994, 1254–1259.

32 J. Pitarch-Jarque, H. R. Jiménez, E. Kalenius, S. Blasco, A. Lopera, M. P. Clares, K. Rissanen and E. García-España, *Dalton Trans.*, 2021, **50**, 9010–9015.

33 C. E. Castillo, J. González-Garcia, J. M. Llinares, M. A. Mañez, H. R. Jiménez, E. García-España and M. G. Basallote, *Dalton Trans.*, 2013, **42**, 6131–6141.

34 B. P. Hay and R. D. Hancock, *Coord. Chem. Rev.*, 2001, **212**, 61–78.

35 A. Bencini, A. Bianchi, P. Paoletti and P. Paoli, *Coord. Chem. Rev.*, 1992, **120**, 51–85.

36 C. Yuste, A. Bentama, S. E. Stiriba, D. Armentano, G. De Munno, F. Lloret and M. Julve, *Dalton Trans.*, 2007, 5190–5200.

37 T. E. Mastropietro, N. Marino, D. Armentano, G. De Munno, C. Yuste, F. Lloret and M. Julve, *Cryst. Growth Des.*, 2013, **13**, 270–281.

38 (*a*) B. J. Hathaway and D. E. Billing, *Coord. Chem. Rev.*, 1970, **5**, 143–202; (*b*) B. J. Hathaway and A. A. G. Tomlinson, *Coord. Chem. Rev.*, 1970, **5**, 1–43.

39 A. W. Addison, T. N. Rao, J. Reedijk, J. van Rijn and G. C. Verschoor, *J. Chem. Soc., Dalton Trans.*, 1984, **7**, 1349–1356.

40 P. M. Wood, *Biochem. J.*, 1988, **253**, 287–289.

41 A. Doménech-Carbó, E. García-España, S. V. Luis, V. Marcelino and J. F. Miravet, *Inorg. Chim. Acta*, 2000, **229**, 238.

42 A. Doménech-Carbó, E. García-España, P. Navarro and C. Miranda, *J. Chem. Soc., Dalton Trans.*, 2006, 4926–4935.

43 L. Guijarro, M. Inclán, J. Pitarh, A. Doménech-Carbó, J. U. Chicote, S. Trefler, E. García-España and B. Verdejo, *Inorg. Chem.*, 2017, **56**, 13748–13758.

44 (*a*) J. M. McCord and I. J. Fridovich, *J. Biol. Chem.*, 1969, **244**, 6049–6055; (*b*) C. Beauchamp and I. J. Fridovich, *Anal. Biochem.*, 1971, **44**, 276–287; (*c*) L. W. Oberley and D. R. Spitz, *Methods Enzymol.*, 1984, **105**, 457–464.

45 C. Gay, J. Collins and J. M. Gebicki, *Redox Rep.*, 1999, **4**, 327–328.

46 L. Iturrino, P. Navarro, I. Rodríguez-Franco, M. Contreras, J. A. Escario, A. Martínez and M. R. Pardo, *Eur. J. Med. Chem.*, 1987, **22**, 445–451.

47 J. Aguilar, P. Díaz, F. Escartí, E. García-España, L. Gil, C. Soriano and B. Verdejo, *Inorg. Chim. Acta*, 2002, **339**, 307–316.

48 E. García-España, M.-J. Ballester, F. Lloret, J. M. Moratal, J. Faus and A. Bianchi, *J. Chem. Soc., Dalton Trans.*, 1988, 101–104.

49 M. Fontanelli and M. Micheloni, *In Proceedings of the First Spanish–Italian Congress on Thermodynamics of Metal Complexes*. Diputación de Castellón, Spain, 1990.

50 G. Gran, *Analyst*, 1952, **77**, 661–672.

51 F. J. C. Rossotti and H. Rossotti, *J. Chem. Educ.*, 1965, **42**, 375–378.

52 W. C. Hamilton, *Statistics in Physical Science. Estimation, Hypothesis Testing, and Least Squares*. The Roland Press Co., New York, 1964.

53 L. Bologni, A. Sabatini and A. Vacca, *Inorg. Chim. Acta*, 1983, **69**, 71–75.

54 H. E. Gottlieb, V. Kotlyar and A. Nudelman, *J. Org. Chem.*, 1997, **62**, 7512–7515.

55 A. K. Covington, M. Paabo, R. A. Robinson and R. G. Bates, *Anal. Chem.*, 1968, **40**, 700–706.

56 O. Dolomanov, O. L. Bourhis, R. Gildea, A. L. Richard, J. A. K. Howard and H. Puschmann, *J. Appl. Crystallogr.*, 2009, **42**, 339–341.

57 G. M. Sheldrick, *Acta Crystallogr., Sect. C: Struct. Chem.*, 2015, **71**, 3–8.

58 J. P. Perdew, *Phys. Rev. B: Condens. Matter Mater. Phys.*, 1986, **33**, 8822–8824.
59 A. D. Becke, *Phys. Rev. A*, 1988, **38**, 3098–3100.
60 C. Lee, W. Yang and R. G. Parr, *Phys. Rev. B: Condens. Matter Mater. Phys.*, 1988, **37**, 785–789.
61 F. Weigend and R. Ahlrichs, *Phys. Chem. Chem. Phys.*, 2005, **7**, 3297–3305.
62 D. Andrae, U. Häußermann, M. Dolg, H. Stoll and H. Preuß, *Theor. Chim. Acta*, 1990, **77**, 123–141.
63 S. Grimme, J. Antony, S. Ehrlich and H. Krieg, *J. Chem. Phys.*, 2010, **132**, 154104.
64 J. Tomasi, B. Mennucci and R. Cammi, *Chem. Rev.*, 2005, **105**, 2999–3093.
65 M. J. Frisch, G. W. Trucks, H. B. Schlegel, G. E. Scuseria, M. A. Robb, J. R. Cheeseman, G. Scalmani, V. Barone, B. Mennucci, G. A. Petersson, *Gaussian 9*, 2009.
66 G. Schaftenaar and J. H. Noordik, *J. Comput. Mol. Des.*, 2000, **14**, 123–134.
67 Schrodinger LLC, *The PyMOL Molecular Graphics System Version 2.0*, (Schrödinger, LLC, 2015), 2015.
68 (*a*) B. H. J. Bielski and H. W. Richter, *J. Am. Chem. Soc.*, 1977, **99**, 3019–3023; (*b*) R. F. Pasternack and B. Halliwell, *J. Am. Chem. Soc.*, 1979, **101**, 1026–1031; (*c*) S. Durot, C. Policar, F. Cisnetti, F. Lambert, J.-P. Renault, G. Pelosi, G. Blain, H. Korri-Youssoufi and J.-P. Mahy, *Eur. J. Inorg. Chem.*, 2005, **2005**, 3513–3523.